JOC The Journal of Organic Chemistry

pubs.acs.org/joc Article

Bromophosphatation as a Mode of Chiral Phosphoric Acid Catalyst Deactivation as Elucidated by Kinetic Profiling

Published as part of The Journal of Organic Chemistry special issue "Physical Organic Chemistry: Never Out of Style".

Ben M. J. Lancaster, Andrew J. P. White, Christopher J. Tighe,* and D. Christopher Braddock*

Cite This: J. Org. Chem. 2025, 90, 6992−7002 Read Online

ABSTRACT: A BINOL-derived chiral phosphoric acid (*R*)-**1** was shown by kinetic profiling to be deactivated during the catalytic bromoesterification of cyclohexene. The products of the deactivation were identified as diastereoisomeric phosphates (*R*,1*R*,2*R*)-**3a** and (*R*,1*S*,2*S*)-**3b** and are formed via an alkene bromophosphatation process where the phosphate of **1** behaves as a competitive nucleophile, as confirmed by authentic preparations of **3a** and **3b** from a stoichiometric bromophosphatation reaction. HPLC separation of the diastereoisomers gave pure **3a** whose absolute and relative configurations were proven by single-crystal X-ray diffraction. The $^{31}P\{^{1}H\}$ NMR spectrum of phosphate **3a** displayed four resonances despite **3a** having just one phosphorus atom, and combined VT-NMR and DFT analysis revealed this to be a consequence of rotational isomerism about the 9-phenanthrene (Ar) bearing C3,3′−Ar bonds. Moreover, kinetic studies using variable time normalization analysis (VTNA) of the catalytic cyclohexene bromoesterification showed first order kinetics in all reactants. The amount of phosphates **3a** and **3b** formed under catalytic bromoesterification conditions was quantified, enabling tracking of the temporal catalyst **1** concentration and hence elucidation of first order kinetics in catalyst **1**. A catalytic cycle consistent with these observations is proposed.

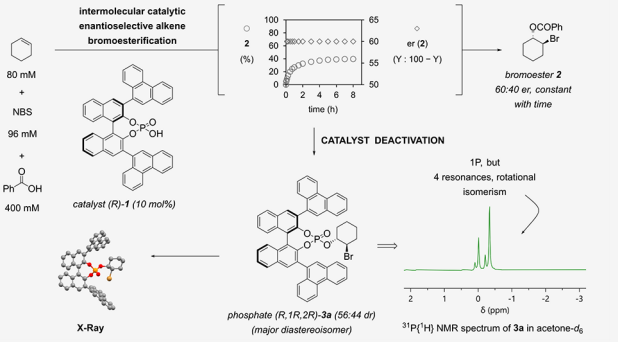

INTRODUCTION

The intermolecular alkene bromoesterification reaction is a direct and versatile approach for the formation of vicinal, stereogenic C−Br and C−O bonds.[1] Since 2007, several examples have been developed using achiral catalysts,[2] but successful enantioselective variants utilizing chiral catalysts remain underdeveloped.[3] In 2012, Tang et al.[3a] reported the first intermolecular, enantioselective alkene bromoesterification reaction utilizing 10 mol % of BINOL-derived chiral phosphoric acid catalyst (*R*)-**1**[4] (Scheme 1). According to Tang et al., various aromatic bromoesters **2**-Ar were prepared in low to moderate er, although in only 10−20% isolated yield. Tang et al. speculated that the low yield might be attributable to a temporal decline in catalyst loading by nucleophilic addition of the phosphate of **1** to a putative bromonium ion. However, no structure was provided for the resultant bromoalkylated phosphate nor were any characterizing data provided.

In 2023, we reported that an intermolecular alkene bromoesterification reaction catalyzed by $(DHQD)_2PHAL$ and utilizing PhCONHBr as the stochiometric electrophilic bromination reagent (as previously reported by Shi et al.)[3c] was inhibited by the benzamide byproduct.[5] Therefore, we considered if inhibition by the succinimide byproduct in Tang et al.'s reaction might be a suitable alternative explanation for the low reaction yields. Herein, we use kinetic profiling methods and time-adjusted analysis to demonstrate that this is not the case and that the phosphoric acid **1** catalyzed bromoesterification of cyclohexene is indeed impeded by deactivation of the catalyst. Moreover, we disclose the preparation of the authentic catalyst deactivation products, to wit, diastereoisomeric phosphates **3a** and **3b** (Figure 1), by the bromoalkylation of phosphoric acid **1**. X-ray diffraction studies of diastereoisomer (*R*,1*R*,2*R*)-**3a** allowed its absolute and relative configurations to be established. Furthermore, the formation of phosphates **3a** and **3b** under standard catalytic bromoesterification conditions was quantified.

Received: February 24, 2025
Revised: April 24, 2025
Accepted: April 28, 2025
Published: May 20, 2025

https://doi.org/10.1021/acs.joc.5c00431
J. Org. Chem. 2025, 90, 6992−7002

Scheme 1. Bromoesterification of Cyclohexene to Form Bromoesters 2-Ar as Reported by Tang et al.[3a]

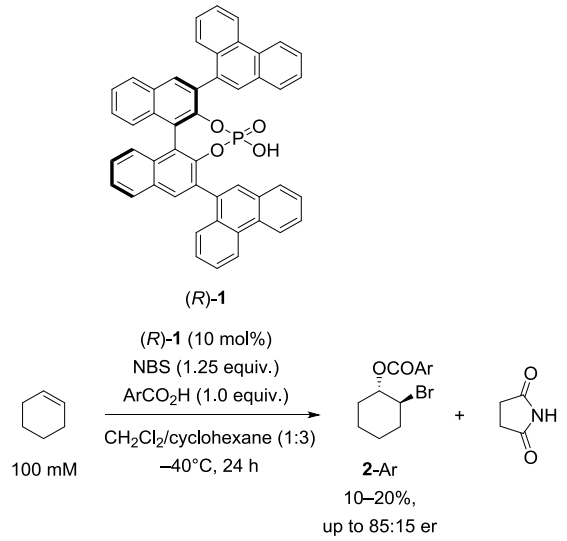

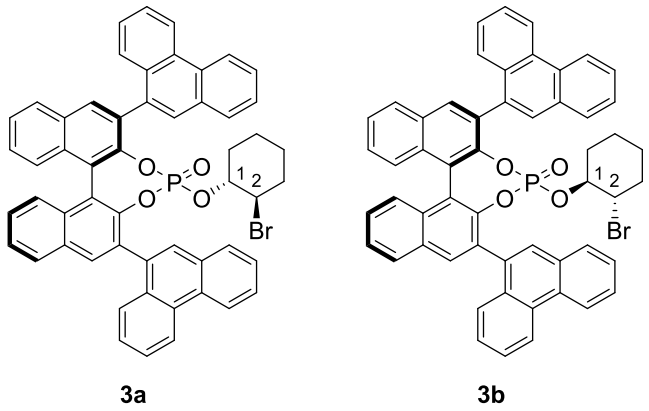

Figure 1. Diastereoisomeric phosphates **3a** and **3b**, which arise from deactivation of Catalyst **1**.

RESULTS AND DISCUSSION

Tang et al.'s phosphoric acid (*R*)-**1** catalyzed bromobenzoylation of cyclohexene with benzoic acid was selected as a representative reaction for kinetic investigation. According to Tang et al., bromoester **2** was isolated in 15% yield and 77.5:22.5 er from a mixture of 1.25 equiv of NBS, 1.0 equiv of benzoic acid and cyclohexene, and 10 mol % of catalyst **1**, in CH_2Cl_2 and cyclohexane (v/v = 1:3, 0.1 M), reacted at −40 °C for 24 h (Scheme 1). However, these conditions did not yield a homogeneous reaction mixture when attempted in our laboratory. Consequently, the first stage of our investigation was to alter the protocol to make the reaction mixture homogeneous and thus amenable to kinetic analysis: the NBS and benzoic acid were adjusted to 1.2 equiv, CH_2Cl_2 was employed as the solvent, the temperature was raised to 0 °C, and the reaction mixture was diluted to 80% of its original concentration. Second, a method was developed to assess the temporal formation of bromoester **2**; viz., aliquots were withdrawn from the reaction, immediately quenched, and analyzed by HPLC with 4,4'-dimethylbenzophenone added as an internal standard.[6] Having developed a protocol for kinetic analysis, an experiment was performed using the specified conditions (Scheme 2). HPLC analysis revealed that after 8 h

Scheme 2. Bromoesterification of Cyclohexene to Form Bromoester 2 Using Modified Conditions

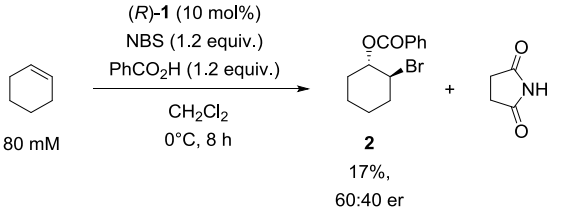

under these conditions, bromoester **2** was formed in 17% conversion and 60:40 er. These results demonstrate a catalytic performance similar to that of Tang et al., albeit with a decrease in er attributable to the increase in temperature, and the bromoesterification is expected to occur in the same mechanistic manifold in both cases.

The final objective before commencing our kinetic study was to raise the conversion to bromoester **2**.[7] Therefore, the influence of benzoic acid on the conversion was investigated by administering an excess of 2.0, 3.5, 5.0, and 10.0 equiv (at 10.0 equiv, the benzoic acid did not fully dissolve). The initial rate of reaction increased in each case as a result, and higher conversions to bromoester **2** were attained over 8 h (Figure 2). Moreover, the er of bromoester **2** in all these reactions remained at 60:40 and did not change with time.[8] The experiment utilizing a 5.0 equiv excess of benzoic acid was

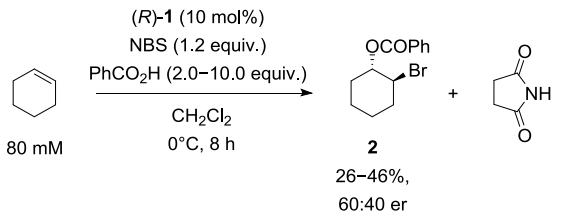

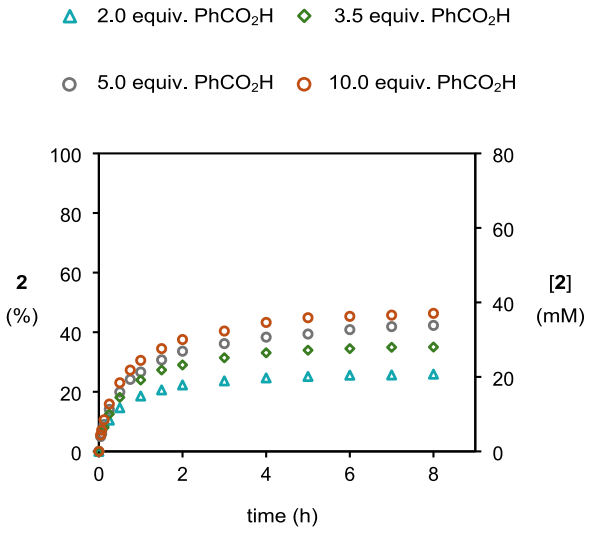

Figure 2. Plot of conversion to **2** (%) and [**2**] vs time in experiments of varying benzoic acid concentrations, as monitored by HPLC methods. $[cyclohexene]_0$ = 80 mM, $[NBS]_0$ = 96 mM, and $[\mathbf{1}]_0$ = 8 mM. (i) △ (blue), with $[PhCO_2H]_0$ = 160 mM. (ii) ◇ (green), with $[PhCO_2H]_0$ = 280 mM. (iii) ○ (gray), with $[PhCO_2H]_0$ = 400 mM. (iv) ○ (orange) (heterogeneous), with $[PhCO_2H]_0$ ~650 mM.

https://doi.org/10.1021/acs.joc.5c00431
J. Org. Chem. 2025, 90, 6992−7002

chosen as the representative standard conditions for subsequent experiments.

To determine if the Brønsted acidity of catalyst **1** was an important attribute of catalysis, an experiment was conducted in which the catalyst was replaced by 10 mol % of the sodium phosphate salt of **1**.[9] HPLC analysis after 8 h indicated that (racemic) bromoester *rac*-**2** formed in just 2% conversion. The same conversion was also obtained on the exclusion of the catalyst from the bromoesterification reaction; evidently, **1** must be in its acidic form for catalysis to proceed. Next, we explored the effect of varying the loading of catalyst **1** (originally 10 mol %) (Figure 3a): when loading was reduced to 6 mol %, the initial reaction rate and conversion to bromoester **2** fell; in contrast, at a greater loading of 20 mol %, the initial reaction rate improved, and an increased conversion to **2** was realized over 8 h.[10]

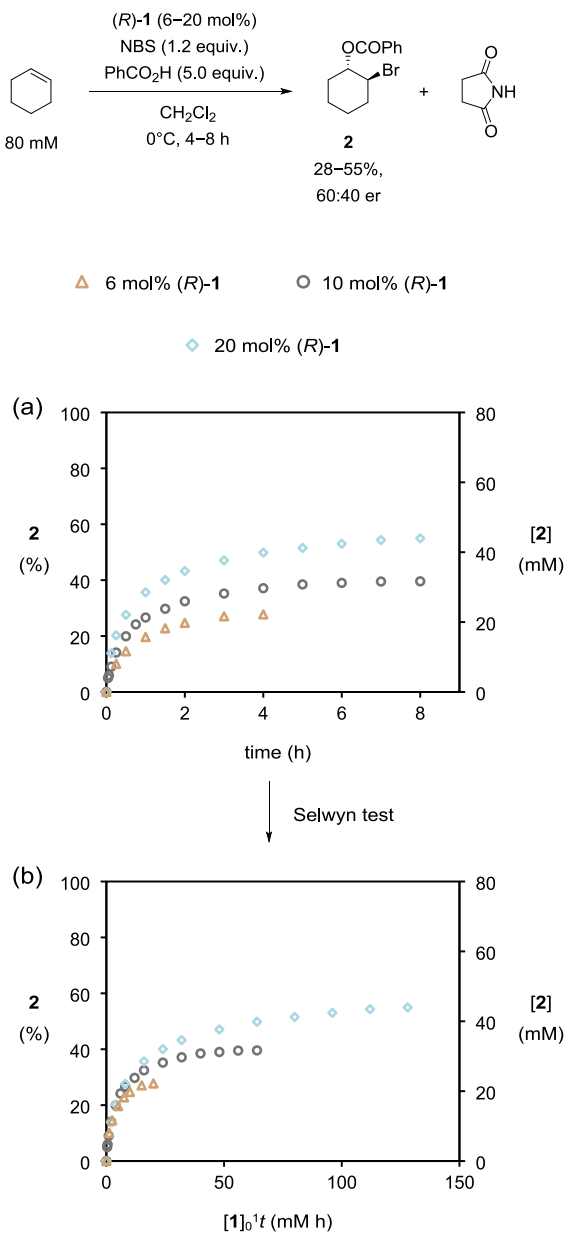

Figure 3. Plots of (a) conversion to **2** (%) and [**2**] vs time and (b) conversion to **2** (%) and [**2**] vs normalized time in experiments with varying catalyst loadings as monitored by HPLC methods. $[\text{cyclohexene}]_0$ = 80 mM, $[PhCO_2H]_0$ = 400 mM, and $[NBS]_0$ = 96 mM. (i) ○ (gray), with $[\mathbf{1}]_0$ = 8 mM. (ii) ◇ (blue), with $[\mathbf{1}]_0$ = 16 mM. (iii) △ (brown), with $[\mathbf{1}]_0$ = 5 mM.

It is apparent from an inspection of the profiles that over half of the conversion to the final bromoester **2** concentration takes place within the first hour, after which the reaction rate slows considerably. Therefore, we were keen to investigate the stability of catalyst **1** by applying the Selwyn test to Figure 3a.[11] Selwyn's test involves recasting the profiles of varying catalyst loading with an abscissa of time multiplied by the initial concentration of **1**. If catalyst **1** is stable, then its concentration will be independent of time, and the normalized profiles will overlay. However, once normalization had been applied, the profiles did not overlay across the full reaction time scale (Figure 3b). This suggests that catalyst **1** is not stable during the reaction and is falling in concentration as the reaction proceeds.[12]

The time-adjusted analysis protocol set forth by Blackmond et al.[13] was utilized to reinforce the finding of catalyst deactivation and to rule out byproduct inhibition. The experiment at 10 mol % catalyst loading was chosen as a representative standard, and a same excess experiment was conducted with initial concentrations of NBS, cyclohexene, and benzoic acid reduced by 20 mM; this simulates 25% completion of the standard experiment, albeit crucially without the presence of products. If neither catalyst deactivation nor product inhibition is occurring, then the same excess plot will overlay with its standard partner once two corrections are applied: (i) adjustment of the same excess time axis by 0.8 h, which corresponds to the time elapsed in the standard experiment for 25% conversion, and (ii) increase of the ordinate by 25% to account for bromoester **2** formed during this time.[14] However, the two profiles did not overlay (Figure 4a), with instead the experiment under the same excess conditions proceeding at faster rate than the standard experiment at the same concentration.

Next, we conducted three iterations of the same excess experiment with the products added: (a) with byproduct succinimide added, (b) with bromoester **2** added, and (c) with both succinimide and **2** added. The profiles (Figure 4b) measured for all three of these experiments did not overlay with the standard experiment but did overlay with the same excess experiment lacking added products. This indicates that neither succinimide nor bromoester **2** depletes the reaction rate and confirms that deactivation of catalyst **1** is responsible for the slowing reaction rate.

Now that the deactivation of the catalyst had been demonstrated—and byproduct inhibition had been excluded—the focus shifted to identifying the product(s) formed by this process. It seemed plausible that the phosphate of **1** could compete with benzoic acid during nucleophilic addition, forming a mixture of (*R*,1*R*,2*R*)-**3a** and (*R*,1*S*,2*S*)-**3b** bromoalkylated phosphate diastereoisomers. Hence, a reaction was devised to form phosphates **3a** and **3b** by reacting a stoichiometric quantity of phosphoric acid **1** with NBS and cyclohexene, in the absence of benzoic acid but under conditions otherwise comparable to our kinetic analyses (Scheme 3). Gratifyingly, from this bromophosphatation process, phosphates **3a** and **3b** were isolated as a mixture in a combined 48% yield.

The HPLC chromatogram of the **3a** and **3b** phosphate mixture, measured with an achiral stationary phase, showed two broad peaks, which integrated to a 56:44 ratio. However,

https://doi.org/10.1021/acs.joc.5c00431
J. Org. Chem. 2025, 90, 6992−7002

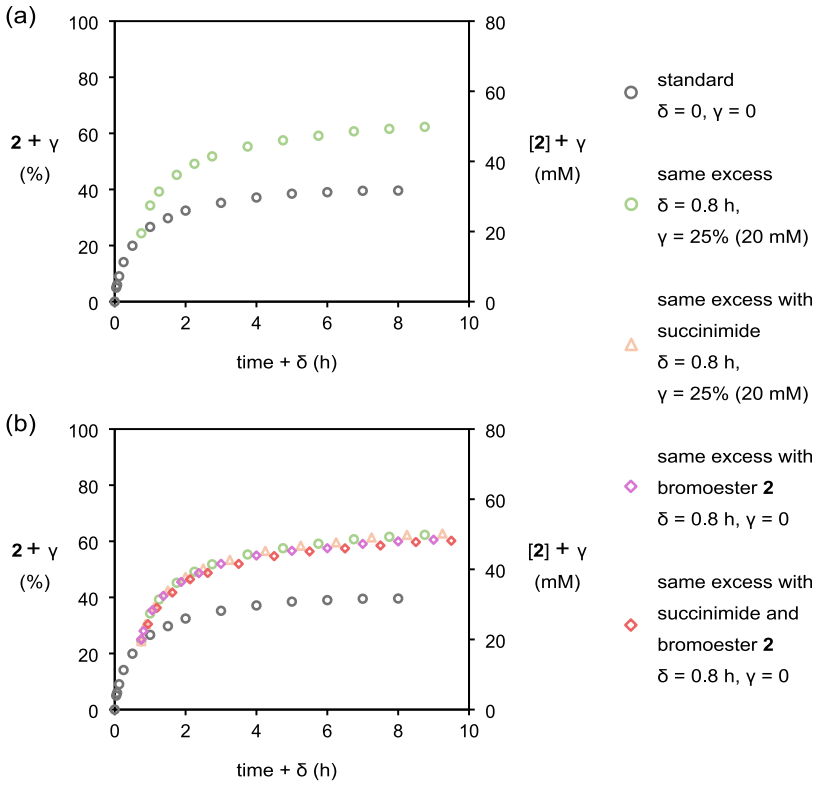

Figure 4. Plot of conversion to **2** (%) and [**2**] vs time in same excess experiments as monitored by HPLC methods. (i) ○ (gray), $[\text{cyclohexene}]_0$ = 80 mM, $[PhCO_2H]_0$ = 400 mM, $[NBS]_0$ = 96 mM, and $[\mathbf{1}]_0$ = 8 mM. (ii) ○ (green), $[\text{cyclohexene}]_0$ = 60 mM, $[PhCO_2H]_0$ = 380 mM, $[NBS]_0$ = 76 mM, and $[\mathbf{1}]_0$ = 8 mM. (iii) △ (orange), as for ○ (green) with $[\text{succinimide}]_0$ = 20 mM. (iv) ◇ (purple), as for ○ (green) with $[rac\text{-}\mathbf{2}]_0$ = 20 mM. (v) ◇ (red), as for ○ (green) with $[\text{succinimide}]_0$ = 20 mM, and $[rac\text{-}\mathbf{2}]_0$ = 20 mM.

Scheme 3. Bromophosphatation of Cyclohexene to Form Bromoalkylated Phosphates 3a and 3b

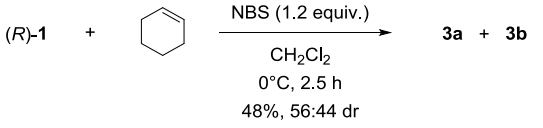

the $^{31}P\{^1H\}$ NMR spectrum of the mixture in acetone-d_6 exhibited 8 resonances (Figure 5). This was unexpected, as each of the phosphates **3a** and **3b** has just one phosphorus atom. Hence, authentic $^{31}P\{^1H\}$ NMR spectra of the purified diastereoisomers were sought for further investigation. The diastereoisomers were inseparable by flash chromatography, although preparative HPLC proved suitable for separation, allowing isolation of pure phosphate diastereoisomer **3a** and 91:9 dr diastereoisomer **3b**. X-ray diffraction measurements of **3a**, following recrystallization by slow diffusion of cyclohexane into a saturated solution in acetone,[15] confirmed its absolute and relative configurations (Figure 6). The $^{31}P\{^1H\}$ NMR spectra of **3a** and **3b** (91:9 dr) (Figure 5) had four (major) resonances each; resonances corresponding to the former diastereoisomer were ∼1 ppm more deshielded than those of the latter. Moreover, when each pair of four resonances was integrated in the $^{31}P\{^1H\}$ NMR spectrum of the mixture, a 56:44 ratio was obtained (Figure 5), directly comparable to the ratio measured by HPLC and therefore confirming this as the dr.

The observation of four resonances in the $^{31}P\{^1H\}$ NMR spectra of each **3a** and **3b** phosphate diastereoisomer could be attributable to hindered rotation about their unsymmetrical 9-phenanthrene groups, giving rise to rotational isomers (Figure 7a). VT $^{31}P\{^1H\}$ NMR studies were conducted to investigate this further. Accordingly, 56:44 dr phosphates **3a** and **3b** in DMSO-d_6 were heated to 100 °C, which caused the seven observable resonances in this solvent at room temperature to collapse into four broad resonances; on cooling, these resonances reverted back to the original seven (for all spectra,

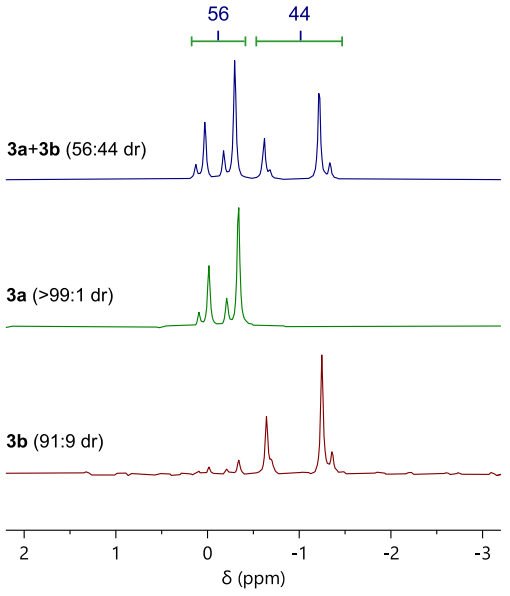

Figure 5. $^{31}P\{^1H\}$ NMR spectra of bromoalkylated phosphates **3a** and **3b** in acetone-d_6.

https://doi.org/10.1021/acs.joc.5c00431
J. Org. Chem. 2025, 90, 6992−7002

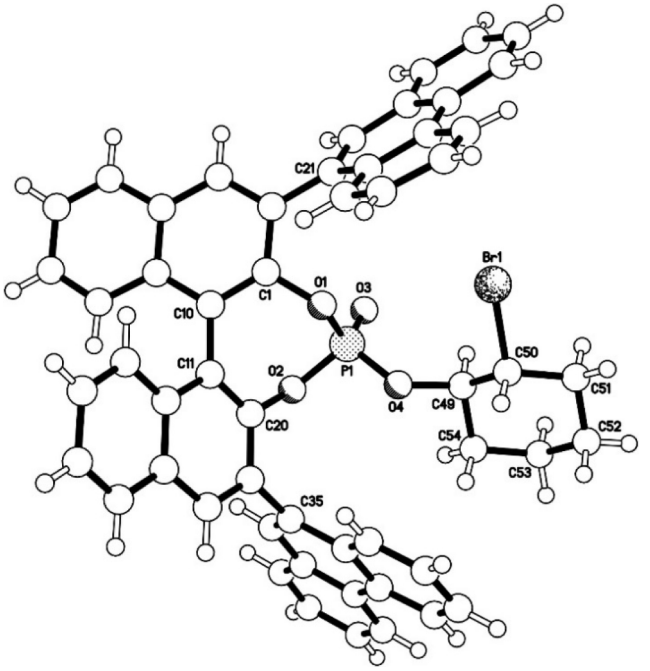

Figure 6. X-ray crystal structure of bromoalkylated phosphate diastereoisomer **3a**.

see the Supporting Information). This experiment demonstrates at least partial conformational exchange on the NMR time scale at this temperature, although operational limitations prevented us from reaching full coalescence at higher temperatures. Therefore, we also opted to conduct DFT studies: in Gaussian 16W, three further orientations of the 9-phenanthrene groups in **3a** were modeled by uploading the X-ray diffraction structure, and adjusting one, or both, torsion angles ω_a and ω_b by 180 degrees. DFT with the B3LYP/IEFPCM/def2-SVP level of theory was used to optimize the structure of each rotamer, and the corresponding potential energies and Boltzmann populations were calculated at 295 K.[16] Gratifyingly, a comparison of the integrals of the four peaks in the $^{31}P\{^1H\}$ NMR spectrum of phosphate **3a** (Figure 7b) with the DFT calculated Boltzmann populations (Figure 7c) shows an excellent match with, at most, a difference of 3% (ii). Therefore, we attribute the four $^{31}P\{^1H\}$ NMR resonances for phosphates **3a** and **3b** to 180-degree rotations about ω_a and ω_b, which occur slowly on the NMR time scale and give rise to 2^2 unique phosphorus environments for each diastereoisomer. This is the first DFT study on rotational isomerism in a 3,3′-diaryl-*O*,*O*′-disubstituted BINOL derivative.[17]

Having isolated and characterized phosphates **3a** and **3b**, they were investigated as possible side products arising from the deactivation of catalyst **1** during the bromoesterification of cyclohexene. Thus, HPLC was utilized to analyze the temporal formation of phosphates **3a** and **3b** simultaneously with bromoester **2** under the standard conditions (Figure 8). Indeed, catalyst **1** underwent bromoalkylation to yield **3a** and **3b**, consuming more than half of catalyst **1** after 1 h and consequently severely retarding the desired enantioselective alkene bromobenzoylation.[18] This result confirms that the low yield of the catalytic bromoesterification of cyclohexene can be attributed to deactivation of phosphoric acid **1** to phosphates **3a** and **3b**. The dr of **3a** and **3b** was 56:44, respectively, and did not vary with time; this is the same ratio as obtained from

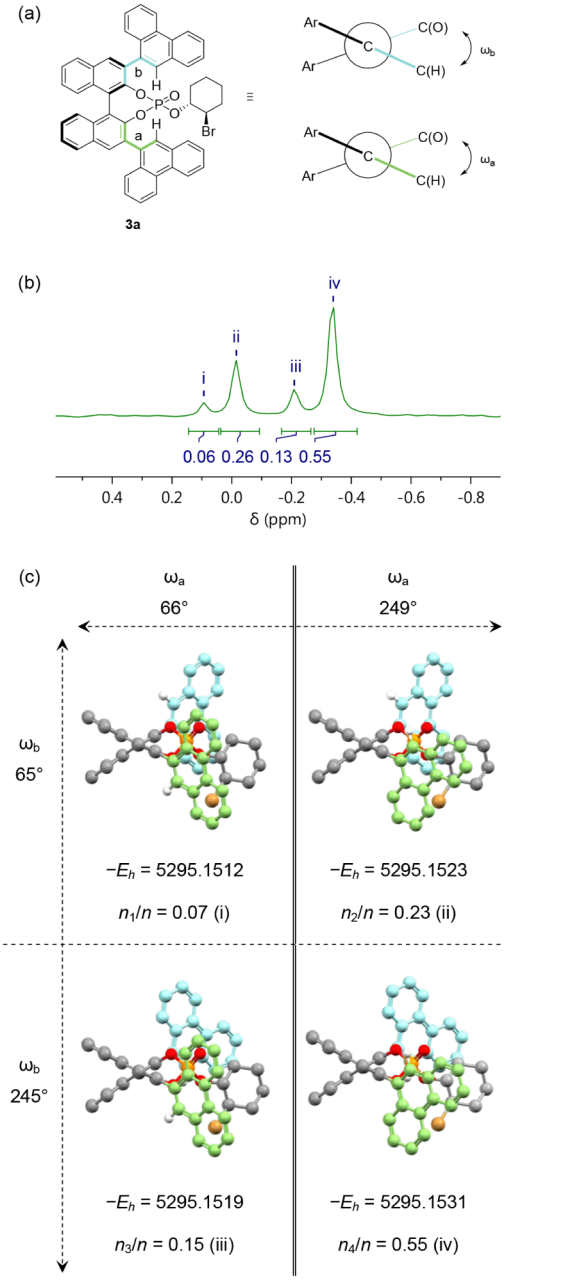

Figure 7. (a) Newman projection of phosphate **3a** with torsion angles ω_a and ω_b defined. (b) $^{31}P\{^1H\}$ NMR spectrum of phosphate **3a** in acetone-d_6 with relative integrals summing to 1P. (c) DFT calculated structures for rotational isomers of phosphate **3a** using the B3LYP/IEFPCM/def2-SVP (acetone) density functional; potential energies (E_h) are provided in Hartree, with Boltzmann populations (n_i/n) expressed summing to 1. ω_a = 249°, ω_b = 65° represents the experimentally determined X-ray diffraction structure.

the bromophosphatation reaction presented earlier in the absence of benzoic acid.

The ability to monitor the deactivation of catalyst **1** enabled a complete kinetic study to determine the orders in the reaction components for the catalytic bromoesterification reaction. Thus, a series of different excess experiments were conducted where the stoichiometry of each reactant was varied (for conditions and all profiles, see the Supporting Information). Burés' variable time normalization analysis (VTNA) procedure was applied to overlay the profiles of

https://doi.org/10.1021/acs.joc.5c00431
J. Org. Chem. 2025, 90, 6992−7002

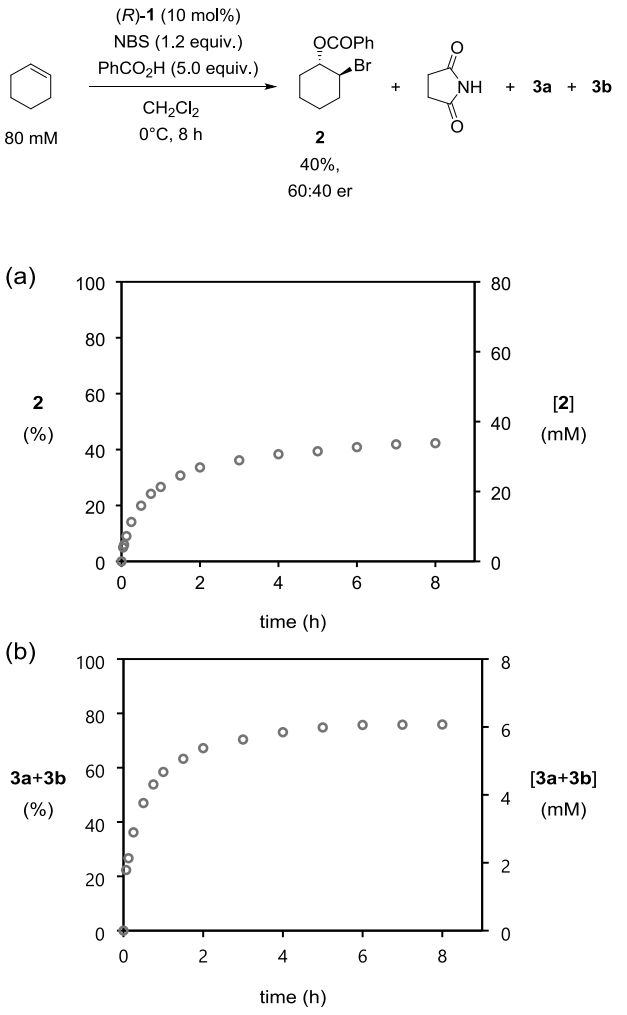

Figure 8. Plots of (a) conversion to **2** (%) and [**2**] vs time and (b) conversion to **3a**+**3b** (%) and [**3a**+**3b**] vs time as monitored by HPLC methods. $[\text{cyclohexene}]_0$ = 80 mM, $[PhCO_2H]_0$ = 400 mM, $[NBS]_0$ = 96 mM, and $[\mathbf{1}]_0$ = 8 mM.

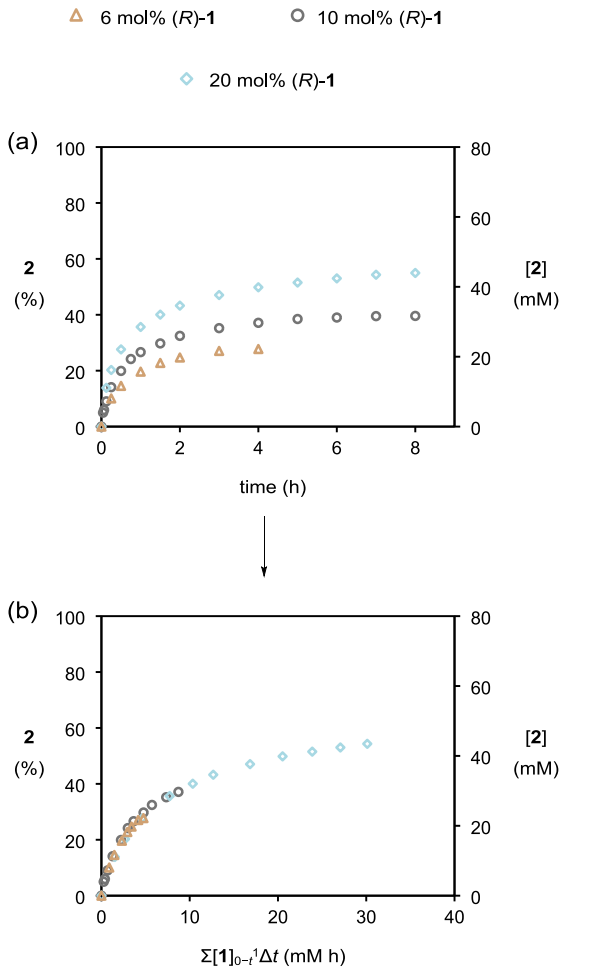

Figure 9. Plots of (a) conversion to **2** (%) and [**2**] vs time and (b) conversion to **2** (%) and [**2**] vs normalized time in experiments with varying catalyst loadings as monitored by HPLC methods. $[\text{cyclohexene}]_0$ = 80 mM, $[PhCO_2H]_0$ = 400 mM, and $[NBS]_0$ = 96 mM. (i) ○ (gray), with $[\mathbf{1}]_0$ = 8 mM. (ii) ◇ (blue), with $[\mathbf{1}]_0$ = 16 mM. (iii) △ (brown), with $[\mathbf{1}]_0$ = 5 mM.

each experiment with the standard partner and hence determine reactant orders.[19] NBS, cyclohexene, and benzoic acid[20] each displayed first order kinetics using this method. The order in catalyst **1** was particularly of interest to validate the existing proposed catalytic cycle,[3a] and so the VTNA method was also applied to our earlier experiments where catalyst **1** loading was varied (Figure 3). To our delight, all three profiles overlaid across the full range when the time scale was normalized with the first power of the temporal catalyst **1** concentration, calculated by subtracting the concentration of phosphates **3a** and **3b** from the initial concentration of **1** (Figure 9). This indicates that catalyst **1** is also first order and supplants the earlier Selwyn analysis. Overall, the VTNA results indicate that NBS, cyclohexene, benzoic acid, and catalyst **1** are involved up to and including the rate-determining step.[21]

To update Tang et al.'s[3a] catalytic cycle based on these findings, we note that List has shown strong heterodimerization between BINOL-derived phosphoric acid (*S*)-TRIP and benzoic acid by NMR spectroscopy, with K_a = 3981 ± 98 M^{-1} in CD_2Cl_2.[22] Hence, we propose herein that the catalyst resting state is heterodimer **4**, which forms through the association of benzoic acid and phosphoric acid **1**, and is particularly likely in our case where the benzoic acid is present in excess (Figure 10). The sodium phosphate salt of **1** does not catalyze the reaction, so catalysis must proceed by reversible proton transfer to NBS (**5**), thereby activating NBS toward reversible electrophilic addition with cyclohexene to form succinimide and to release putative bromonium ion **8** into the electrostatically charge-neutral bulk solution. The weak association of a second carboxylic acid to phosphate **6**—favored by an increase in carboxylic acid concentration—would facilitate subsequent formation of bromoester **2** in a chiral catalyst environment and close the cycle to heterodimer **4**. Alternatively, bromoalkylation of phosphate **6** would give deactivated products **3a** and **3b**.[23]

CONCLUSIONS

In conclusion, we have demonstrated that BINOL-derived chiral phosphoric acid (*R*)-**1** deactivates to bromoalkylated phosphates **3a** and **3b** during the catalytic bromoesterification of cyclohexene. These phosphates were synthesized authentically in an experiment in which the benzoic acid nucleophile was absent. This constitutes the first characterized example of an alkene bromophosphatation process, wherein the phosphate of **1** takes the role of a nucleophile to a putative bromonium

https://doi.org/10.1021/acs.joc.5c00431
J. Org. Chem. 2025, 90, 6992−7002

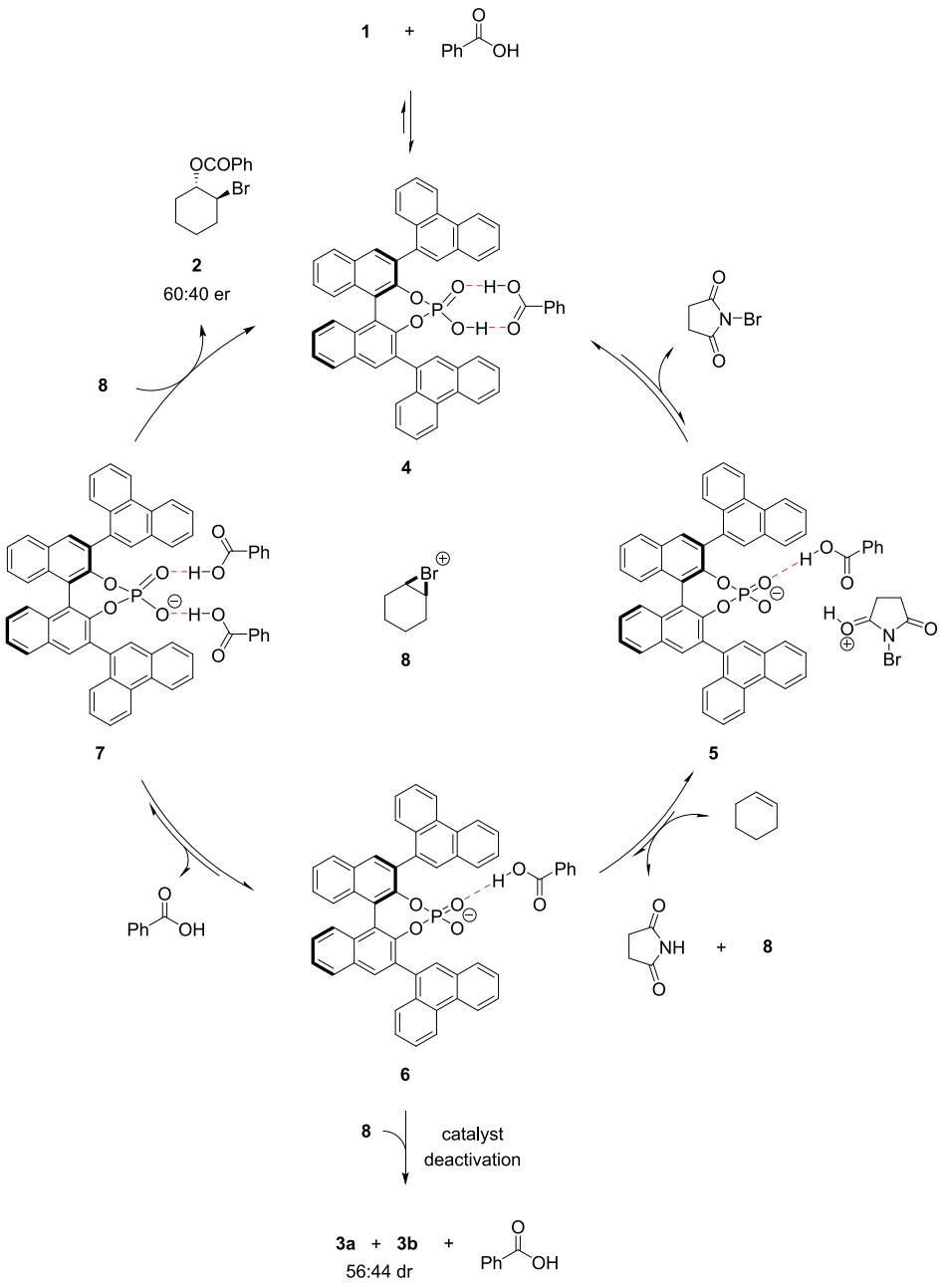

Figure 10. Proposed mechanism for the bromoesterification of cyclohexene.

ion.[22c,24] $^{31}P\{^{1}H\}$ NMR and DFT studies revealed that both phosphates **3a** and **3b** exhibit rotational isomerism with respect to 180-degree rotations about their 9-phenanthrene (Ar) bearing C3,3′−Ar bonds. X-ray diffraction studies were conducted on phosphate **3a** after preparative HPLC separation from **3b** and provided proof of absolute and relative configuration. VTNA studies determined that the catalytic bromoesterification of cyclohexene is first order in all of the reacting components and catalyst **1**, and an updated catalytic cycle has been presented. It is expected that these studies will aid the design of new chiral phosphoric acid derivatives which circumvent deactivation in enantioselective alkene halofunctionalization reactions.[25]

EXPERIMENTAL SECTION

General Experimental Methods. NBS was recrystallized from H_2O before use, and cyclohexene was distilled before use. Phosphoric acid (*R*)-**1** was prepared following our recommended procedure and was acidified with aqueous 6 M HCl before use.[4a] All other reagents and commercial grade solvents were utilized without further purification. Flash chromatography used Geduran Si 60, particle size 40−63 μm. Thin layer chromatography (TLC) used Merck Kieselgel 60 F_{254} precoated aluminum-backed plates. The developed plates were visualized by irradiation with UV light (254 or 366 nm) or staining with a $KMnO_4$ solution.

^{1}H, $^{13}C\{^{1}H\}$, and $^{31}P\{^{1}H\}$ NMR spectra were recorded by using a Bruker AV-400 NMR spectrometer. All chemical shifts (δ) are expressed in ppm (parts per million) relative to the residual solvent peak. Abbreviations for multiplicities are s,

https://doi.org/10.1021/acs.joc.5c00431
J. Org. Chem. 2025, 90, 6992−7002

singlet; d, doublet; t, triplet; m, multiplet; app, apparent. Fourier transform infrared (IR) spectra were recorded neat on an ATR-IR spectrometer. Mass spectra were recorded by the Imperial College Department of Chemistry Mass Spectroscopy Service. Melting points were recorded using an OptiMelt MPA100 apparatus. Optical rotations were measured on an ADP 440+ polarimeter with a path length of 0.5 dm using the D-line of sodium; concentrations (c) are provided in g/100 mL. X-ray crystallography of bromoalkylated phosphate **3a** was conducted by the Imperial College Department of Chemistry X-ray Crystallography Facility with an Agilent Xcalibur PX Ultra A diffractometer. HPLC separations were performed using PerkinElmer Series 200 or Agilent 1260 Infinity II HPLC systems, and the enantiopurity of bromoester **2** was established by HPLC following comparison to an authentic racemic sample. All kinetic bromoesterification experiments were conducted twice or more, and the resulting profiles were averaged between runs.

Standard Procedure for Cyclohexene Bromoesterification. NBS (51.3 mg, 0.288 mmol) and phosphoric acid **1** (16.8 mg, 0.0240 mmol) were added to an oven-dried, single-necked flask. $PhCO_2H$ (2.80 mL, 0.429 M in CH_2Cl_2, 1.20 mmol) and $(4\text{-Tol})_2CO$ (0.200 mL, 0.600 M in CH_2Cl_2, 0.120 mmol) were injected in the flask, and the solution was stirred at 350 rpm until homogeneous. The solution was cooled to 0 °C and after 10 min, cyclohexene (24.3 μL, 0.240 mmol) was added to begin the experiment. The reaction mixture was sampled (25 μL) at the specified time, and the solution was transferred to a vial containing saturated aqueous $Na_2S_2O_3$ (200 μL) and MeCN (200 μL). The biphasic mixture was shaken for 30 s, and the top layer was removed and filtered over a cotton packed pipet containing silica gel (∼120 mg) into a HPLC vial. MeCN (300 μL) was eluted through silica into the HPLC vial. [**2**], [**3a**+**3b**], and dr (**3a**+**3b**) were determined by HPLC (SUPELCOSIL LC-18), 50−40−10% H_2O in MeCN, 1.0 mL/min, λ = 230 nm, R_t ($(4\text{-Tol})_2CO$) = 6.8 min, R_t (**2**) = 8.7 min, R_t (**3a**) = 22.5 min, R_t (**3b**) = 24.0 min. The lids of the vials were unscrewed, and the solvent was left to evaporate. The resulting residue was redissolved in 5% IPA in n-hexane (1 mL). er (**2**) was determined by HPLC (CHIRALPAK-AD), 0.5% IPA in n-hexane, 1.0 mL/min, λ = 230 nm, R_t (1S,2S)-**2** = 9.1 min, and R_t (1R,2R)-**2** = 10.1 min. Other experiments where the initial concentrations of catalyst **1**, NBS, cyclohexene, or $PhCO_2H$ were varied were conducted by using the above procedure with adjustments to the stoichiometry as specified.

Same Excess Procedure for Cyclohexene Bromoesterification. NBS (40.6 mg, 0.228 mmol) and phosphoric acid **1** (16.8 mg, 0.0240 mmol) were added to an oven-dried, single-necked flask. CH_2Cl_2 (0.140 mL) **or** bromoester *rac*-**2** (0.140 mL, 0.429 M in CH_2Cl_2, 0.060 mmol), then $PhCO_2H$ (2.66 mL, 0.429 M in CH_2Cl_2, 1.14 mmol) **or** $PhCO_2H$ + succinimide (2.66 mL, 0.429 M + 0.0226 M in CH_2Cl_2, 1.14 mmol + 0.0600 mmol) and $(4\text{-Tol})_2CO$ (0.200 mL, 0.600 M in CH_2Cl_2, 0.120 mmol) were injected in the flask, and the solution was stirred at 350 rpm until homogeneous. The solution was cooled to 0 °C, and after 10 min, cyclohexene (18.2 μL, 0.180 mmol) was added. The reaction mixture was sampled and analyzed as above.

*(1S,2S)-(+)-2-Bromocyclohexyl Benzoate (**2**).* NBS (51.3 mg, 0.288 mmol) and phosphoric acid **1** (16.8 mg, 0.0240 mmol) were added to an oven-dried, single-necked flask. $PhCO_2H$ (2.80 mL, 0.429 M in CH_2Cl_2, 1.20 mmol) and CH_2Cl_2 (0.200 mL) were injected in the flask, and the solution was stirred at 350 rpm until homogeneous. The solution was cooled to 0 °C and after 10 min, cyclohexene (24.3 μL, 0.240 mmol) was added. After 8 h, the reaction mixture was washed with saturated aqueous $Na_2S_2O_3$ (5 mL), the layers were separated, and the aqueous phase was extracted with CH_2Cl_2 (3 × 5 mL). The combined organics were dried over $MgSO_4$, filtered and concentrated *in vacuo*. The resulting residue was chromatographed (3% EtOAc in petroleum ether) to provide bromoester **2** (17.8 mg, 26%) as a colorless oil. R_f = 0.40 (3% EtOAc in petroleum ether); $[\alpha]_D^{24}$ = +20.2 (c = 0.89, $CHCl_3$) (lit.[26] $[\alpha]_D^{24}$ = +104.6, c = 1.0, $CHCl_3$, 95:5 er); IR (film) 1712 cm^{-1}; ^1H NMR (400 MHz, $CDCl_3$) δ 8.09−8.06 (m, 2H), 7.57 (app t, J = 7.6 Hz, 1H), 7.45 (app t, J = 7.6 Hz, 2H), 5.13 (ddd, J = 9.2, 9.1, 4.4 Hz, 1H), 4.16 (ddd, J = 10.4, 9.1, 4.4 Hz, 1H), 2.45−2.38 (m, 1H), 2.32−2.23 (m, 1H), 1.95 (dddd, J = 17.1, 11.2, 7.3, 3.9 Hz, 1H), 1.86−1.74 (m, 2H), 1.58−1.34 (m, 3H); $^{13}C\{^1H\}$ NMR (101 MHz, $CDCl_3$) δ 165.7, 133.2, 130.4, 129.8, 128.5, 76.5, 52.8, 35.7, 31.2, 25.5, 23.4; HRMS (APCI$^+$, ion trap) calcd. for $C_{13}H_{15}O_2$ (M−Br)$^+$, 203.1067; found, 203.1059; HPLC (CHIRALPAK-AD), 0.5% IPA in n-hexane, 1.0 mL/min, λ = 230 nm, R_t (1S,2S)-**2** = 9.1 min, and R_t (1R,2R)-**2** = 10.1 min (59:41 er).

Bromophosphatation of Cyclohexene. *Bromocyclohexyl Phosphate (R,1R,2R)-**3a** and Bromocyclohexyl Phosphate (R,1S,2S)-**3b**.* Cyclohexene (4.1 μL, 0.040 mmol) was added to a stirred solution of NBS (8.5 mg, 0.048 mmol) and phosphoric acid **1** (28.0 mg, 0.0400 mmol) in CH_2Cl_2 (0.5 mL) at 0 °C. After 2.5 h, the cloudy reaction mixture was directly chromatographed (CH_2Cl_2) to provide phosphates **3a** +**3b** (16.7 mg, 48%) as a white solid. R_f = 0.80 (CH_2Cl_2); mp. 200 °C (dec.); IR (film) 1295 cm^{-1}; ^1H NMR (400 MHz, acetone-d_6) δ 8.95−8.79 (m, 4H), 8.42−8.13 (m, 4H), 8.08−7.91 (m, 4H), 7.90−7.40 (m, 16H), 3.64−3.48 (m, 0.74H), 3.42−3.19 (m, 0.73H), 3.16−3.10 (m, 0.32H), 2.74−2.68 (m, 0.16H), 2.28−2.11 (m, 0.23H), 1.81−0.21 (m, 8.49H), −0.97−−1.08 (m, 0.18H); $^{13}C\{^1H\}$ NMR (101 MHz, acetone-d_6) δ 206.1, 147.1, 145.9, 135.4, 135.1, 134.6, 134.4, 134.3, 134.2, 134.0, 133.6, 133.49, 133.45, 133.4, 133.2, 133.0, 132.8, 132.6, 132.50, 132.45, 132.1, 132.0, 131.9, 131.8, 131.43, 131.36, 131.3, 131.2, 131.02, 130.97, 130.8, 130.7, 130.4, 130.2, 130.1, 129.9, 129.74, 129.68, 129.64, 129.59, 128.3, 128.12, 128.07, 128.02, 127.98, 127.93, 127.87, 127.83, 127.79, 127.7, 127.64, 127.55, 127.5, 127.4, 127.32, 127.25, 127.2, 124.0, 123.82, 123.76, 123.7, 123.6, 123.52, 123.46, 123.4, 123.0, 122.4, 122.2, 83.5, 83.1, 82.1, 52.2, 51.7, 32.1, 31.2, 25.3, 24.8, 23.1, 22.9, 21.9; $^{31}P\{^1H\}$ NMR (162 MHz, acetone-d_6) δ 0.1 (**3a**), 0.0 (**3a**), −0.2 (**3a**), −0.3 (**3a**), −0.6 (**3b**), −0.7 (**3b**), −1.2 (**3b**), −1.3 (**3b**) (multiple signals due to the presence of rotamers); HRMS (ESI$^+$, TOF) calcd. for $C_{54}H_{39}{}^{79}BrO_4P$ (M+H)$^+$, 861.1764; found, 861.1760; HPLC (SUPELCOSIL LC-18), 10% H_2O in MeCN, 1.0 mL/min, λ = 230 nm, R_t (**3a**) = 9.1 min, R_t (**3b**) = 10.5 min (56:44 dr); HPLC (CHIRALPAK-AD), 20% IPA in n-hexane, 1.0 mL/min, λ = 230 nm, R_t (**3a**) = 6.9 min, R_t (**3b**) = 9.2 min (both diastereoisomers >99:1 er). HPLC was used to preparatively separate the **3a** and **3b** diastereoisomers, providing pure phosphates **3a** (5.5 mg) and **3b** (3.9 mg, 91:9 dr) as white solids, after 20 runs. HPLC (Poroshell 120 SB-C18), 100% MeCN, 25 mL/min, λ = 250 nm, 400 μL injection, 3 mg/mL sample concentration in MeCN, R_t (**3a**) = 3.7 min, and R_t (**3b**) = 3.9 min. Crystal data for **3a**: $C_{54}H_{38}BrO_4P{\cdot}2.25$-

https://doi.org/10.1021/acs.joc.5c00431
J. Org. Chem. 2025, 90, 6992−7002

(C_6H_{12}), M = 1051.07, orthorhombic, $P2_12_12_1$ (no. 19), a = 8.4319(3), b = 20.6529(6), c = 31.3293(8) Å, V = 5455.8(3) Å^3, Z = 4, D_c = 1.280 g cm^{-3}, μ(Mo−Kα) = 0.833 mm^{-1}, T = 173 K, colorless tablets, Agilent Xcalibur 3 E diffractometer; 10,763 independent measured reflections (R_{int} = 0.0264), F^2 refinement,[27] R_1(obs) = 0.0476, wR_2(all) = 0.1066, 8210 independent observed absorption-corrected reflections [$|F_0| > 4\sigma(|F_0|)$, completeness to θ_{full}(25.2°) = 99.4%], 541 parameters. The absolute configuration of phosphate **3a** was determined by the use of the Flack parameter [x^+ = 0.007(4)]. CCDC 2395133.

■ ASSOCIATED CONTENT

Data Availability Statement

The data underlying this study are available in the published article, in its Supporting Information, and openly available in the Imperial College research data repository at 10.14469/hpc/14708.

Supporting Information

The Supporting Information is available free of charge at https://pubs.acs.org/doi/10.1021/acs.joc.5c00431.

HPLC calibration method; representative HPLC chromatograms; different excess experiments; X-ray structure of phosphate **3a**; calculation of Boltzmann populations; variable temperature $^{31}P\{^1H\}$ NMR experiment; and copies of ^1H, $^{13}C\{^1H\}$, and $^{31}P\{^1H\}$ NMR spectra (PDF)

Accession Codes

Deposition Number 2395133 contains the supplementary crystallographic data for this paper. These data can be obtained free of charge via the joint Cambridge Crystallographic Data Centre (CCDC) and Fachinformationszentrum Karlsruhe Access Structures service.

■ AUTHOR INFORMATION

Corresponding Authors

D. Christopher Braddock − *Department of Chemistry, Imperial College London, Molecular Sciences Research Hub, London W12 0BZ, U.K.*; orcid.org/0000-0002-4161-7256; Email: c.braddock@imperial.ac.uk

Christopher J. Tighe − *Department of Chemical Engineering, Imperial College London, South Kensington Campus, London SW7 2AZ, U.K.*; orcid.org/0000-0002-0483-7698; Email: c.tighe@imperial.ac.uk

Authors

Ben M. J. Lancaster − *Department of Chemistry, Imperial College London, Molecular Sciences Research Hub, London W12 0BZ, U.K.*; orcid.org/0000-0002-5638-3333

Andrew J. P. White − *Department of Chemistry, Imperial College London, Molecular Sciences Research Hub, London W12 0BZ, U.K.*

Complete contact information is available at: https://pubs.acs.org/10.1021/acs.joc.5c00431

Author Contributions

D.C.B., C.J.T., and B.M.J.L. conceptualized the project. B.M.J.L. devised and performed the experimental procedures. A.J.P.W. conducted X-ray crystal structure determinations. D.C.B. and C.J.T. supervised the project. B.M.J.L. wrote the original draft, and all edited to the final version.

Notes

The authors declare no competing financial interest.

■ ACKNOWLEDGMENTS

The authors thank the EPSRC Centre for Doctoral Training in Next Generation Synthesis and Reaction Technology (Imperial College London, EP/S023232/1) for a studentship to B.M.J.L.

■ REFERENCES

(1) For comprehensive reviews on catalytic, enantioselective alkene bromofunctionalization reactions including bromoesterification, see: (a) Denmark, S. E.; Kuester, W. E.; Burk, M. T. Catalytic Asymmetric Halofunctionalization of Alkenes—A Critical Perspective. *Angew. Chem., Int. Ed.* **2012**, *51*, 10938−10953. (b) Tan, C. K.; Yeung, Y.-Y. Recent Advances in Stereoselective Bromofunctionalization of Alkenes using *N*-Bromoamide Reagents. *Chem. Commun.* **2013**, *49* (73), 7985−7996. (c) Cheng, Y. A.; Yu, W. Z.; Yeung, Y.-Y. Recent Advances in Asymmetric Intra- and Intermolecular Halofunctionalizations of Alkenes. *Org. Biomol. Chem.* **2014**, *12* (15), 2333−2343. (d) Chen, J.; Zhou, L. Recent Progress in the Asymmetric Intermolecular Halogenation of Alkenes. *Synthesis* **2014**, *46*, 586−595. (e) Yan, J.; Zhou, Z.; He, Q.; Chen, G.; Wei, H.; Xie, W. The Applications of Catalytic Asymmetric Halocyclization in Natural Product Synthesis. *Org. Chem. Front.* **2022**, *9*, 499−516.

(2) For examples of intermolecular alkene bromoesterification reactions using achiral catalysts, see: (a) Ahmad, S. M.; Braddock, D. C.; Cansell, G.; Hermitage, S. A. Dimethylformamide Dimethylacetamide and Tetramethylguanidine as Nucleophilic Organocatalysts for the Transfer of Electrophilic Bromine from *N*-Bromosuccinimide to Alkenes. *Tetrahedron Lett.* **2007**, *48*, 915−918. (b) Ahmad, S. M.; Braddock, D. C.; Cansell, G.; Hermitage, S. A.; Redmond, J. M.; White, A. J. P. Amidines as Potent Nucleophilic Organocatalysts for the Transfer of Electrophilic Bromine from *N*-Bromosuccinimide to Alkenes. *Tetrahedron Lett.* **2007**, *48*, 5948−5952. (c) Shi, Y.; Wong, J.; Ke, Z.; Yeung, Y.-Y. Lipophilic Indole-Catalyzed Intermolecular Bromoesterification of Olefins in Nonpolar Media. *J. Org. Chem.* **2019**, *84* (7), 4017−4024. (d) Wan, C.; Song, R.-J.; Li, J.-H. Electrooxidative 1,2-Bromoesterification of Alkenes with Acids and *N*-Bromosuccinimide. *Org. Lett.* **2019**, *21* (8), 2800−2803. (e) Ng, W.-H.; Hu, R.-B.; Lam, Y.-P.; Yeung, Y.-Y. Zwitterion-Catalyzed Intermolecular Bromoesterifications. *Org. Lett.* **2020**, *22* (14), 5572−5576. (f) Wong, J.; Yeung, Y.-Y. Solvent and Catalyst-Free Bromofunctionalization of Olefins using a Mechanochemical Approach. *RSC Adv.* **2021**, *11* (22), 13564−13570. (g) Moriyama, K.; Kuramochi, M.; Tsuzuki, S.; Fujii, K.; Morita, T. Nitroxyl Catalysts for Six-Membered Ring Bromolactonization and Intermolecular Bromoesterification of Alkenes with Carboxylic Acids. *Org. Lett.* **2021**, *23* (2), 268−273. (h) Yang, J.; Chan, Y.-Y.; Feng, W.; Tse, Y.-L. S.; Yeung, Y.-Y. Study and Applications of Tetrasubstituted Hypervalent Selenium−Halogen Species in Catalytic Electrophilic Halogenations. *ACS Catal.* **2023**, *13*, 2386−2395.

(3) For examples of intermolecular, enantioselective alkene bromoesterification reactions using chiral catalysts, see: (a) Li, G.-X.; Fu, Q.-Q.; Zhang, X.-M.; Jiang, J.; Tang, Z. First Asymmetric Intermolecular Bromoesterification Catalyzed by Chiral Brønsted Acid. *Tetrahedron: Asymmetry* **2012**, *23* (3−4), 245−251. (b) Zhang, W.; Liu, N.; Schienebeck, C. M.; Zhou, X.; Izhar, I. I.; Guzei, I. A.; Tang, W. Enantioselective Intermolecular Bromoesterification of Allylic Sulfonamides. *Chem. Sci.* **2013**, *4* (6), 2652−2656. (c) Li, L.; Su, C.; Liu, X.; Tian, H.; Shi, Y. Catalytic Asymmetric Intermolecular Bromoesterification of Unfunctionalized Olefins. *Org. Lett.* **2014**, *16*, 3728−3731.

(4) For our recommended procedure on the synthesis of BINOL-derived chiral phosphoric acid **1**, see: (a) Lancaster, B. M. J.; White, A. J. P.; Braddock, D. C. Fortuitous Enantiomeric Self-Rectification of an Unreported Partial Racemisation in the Synthesis of a Chiral Phosphoric Acid: A Warning to Practitioners. *Chem.- Eur. J.* 2024, *30*,

e202403318. For a comprehensive review on BINOL-derived chiral phosphoric acids, see: (b) Parmar, D.; Sugiono, E.; Raja, S.; Rueping, M. Complete Field Guide to Asymmetric BINOL-Phosphate Derived Brønsted Acid and Metal Catalysis: History and Classification by Mode of Activation; Brønsted Acidity, Hydrogen Bonding, Ion Pairing, and Metal Phosphates. *Chem. Rev.* **2014**, *114*, 9047−9153.
(5) Braddock, D. C.; Lancaster, B. M. J.; Tighe, C. J.; White, A. J. P. Surmounting Byproduct Inhibition in an Intermolecular Catalytic Asymmetric Alkene Bromoesterification Reaction as Revealed by Kinetic Profiling. *J. Org. Chem.* **2023**, *88*, 8904−8914.
(6) $(4\text{-Tol})_2CO$ was added into all kinetic experiments at 40 mM concentration, and was confirmed to not influence the reaction rate (see the Supporting Information).
(7) Blackmond has recommended that visual kinetic analyses are carried out between 15−85% conversion of the limiting substrate: Blackmond, D. G. Reaction Progress Kinetic Analysis: A Powerful Methodology for Mechanistic Studies of Complex Catalytic Reactions. *Angew. Chem. Int. Ed.* 2005, *44*, (28), 4302−4320.
(8) The er of **2** rose slightly from 58:42 at 5 min to 60:40 at 15 min, and then remained constant; however, the rise may not be significant due to difficulties in integrating the HPLC peaks of bromoesters (1*S*,2*S*)-**2** and (1*R*,2*R*)-**2** during early stages of the reaction, where conversion is low.
(9) Phosphoric acid **1** (53.9 mg, 0.0769 mmol) was neutralized into sodium phosphate (53.0 mg, 95%) following a general literature procedure (without subsequent recrystallization): Hennecke, U.; Müller, C. H.; Fröhlich, R. Enantioselective Haloetherification by Asymmetric Opening of *meso*-Halonium Ions. *Org. Lett.* **2011**, *13*, 860−863.
(10) Here, the er of bromoester **2** was 60:40, and the dr of phosphates **3a** and **3b** (*vide infra*) was 56:44, respectively. These values did not significantly change when the catalyst loading, or equivalents of benzoic acid, were varied, and both remained constant with time.
(11) Selwyn, M. J. A Simple Test for Inactivation of an Enzyme During Assay. *Biochim. Biophys. Acta, Enzymol. Biol. Oxid.* **1965**, *105*, 193−195.
(12) The absence of overlay could also be justified by nonfirst order kinetics in catalyst **1**; however, **1** is shown to indeed be of first order (*vide infra*).
(13) For instructional detail on the time-adjusted analysis technique, see: Baxter, R. D.; Sale, D.; Engle, K. M.; Yu, J.-Q.; Blackmond, D. G. Mechanistic Rationalization of Unusual Kinetics in Pd-Catalyzed C−H Olefination. *J. Am. Chem. Soc.* **2012**, *134*, 4600−4606.
(14) Most frequently, same excess plots are expressed as the depleting concentration of starting material vs time, and the ordinate correction applied here is not required.
(15) These conditions did not give X-ray quality crystals when attempted with 56:44 dr phosphates **3a** and **3b**, demonstrating the value of prior separation of the diastereoisomers.
(16) See the Supporting Information for details on the calculation of Boltzmann populations.
(17) NMR spectra of unsymmetrical 3,3′-diaryl-*O*,*O*′-disubstituted BINOL derivatives have been reported as complex: For Ar = 1-naphthyl, 9-phenanthrenyl, *O*R,*O*′R = *N*-triflyl phosphoramide, *N*-mesyl phosphoramide, see: (a) Zhao, P.; Cheng, A.; Wang, X.; Ma, J.; Zhao, G.; Li, Y.; Zhang, Y.; Zhao, B. Asymmetric Intramolecular Hydroalkoxylation of Unactivated Alkenes Catalyzed by Chiral Triflyl Phosphoramide and $TiCl_4$. *Chin. J. Chem.* **2020**, *38*, 565−569. (b) For Ar = 9-phenanthrenyl, *O*R,*O*′R = bis(*N*,*N*-dimethylthiocarbamate), see: Gatzenmeier, T.; van Gemmeren, M.; Xie, Y.; Höfler, D.; Leutzsch, M.; List, B. Asymmetric Lewis Acid Organocatalysis of the Diels−Alder reaction by a Silylated C−H Acid. *Science* **2016**, *351*, 949−952. (c) For Ar = 1-naphthyl, 2-isopropylphenyl, 2-isopropyl-5-methylphenyl, *O*R,*O*′R = diol, dimethoxy ether, phosphorochloridate, phosphoramidate, iminodiphosphate, see: Kim, J. H.; Čorić, I.; Vellalath, S.; List, B. The Catalytic Asymmetric Acetalization. *Angew. Chem., Int. Ed.* **2013**, *52*, 4474−4477. (d) For Ar = 2-cyclohexyl-5-methylphenyl, *O*R,*O*′R = diol, dimethoxy ether, phosphorochloridate, phosphoramidate, iminodiphosphate, see: Kim, J. H.; Čorić, I.; Palumbo, C.; List, B. Resolution of Diols via Catalytic Asymmetric Acetalization. *J. Am. Chem. Soc.* **2015**, *137*, 1778−1781. (e) For Ar = 1-naphthyl, *O*R,*O*′R = dimethoxymethyl ether, see: Le Saux, E.; Georgiou, E.; Dmitriev, I. A.; Hartley, W. C.; Melchiorre, P. Photochemical Organocatalytic Functionalization of Pyridines via Pyridinyl Radicals. *J. Am. Chem. Soc.* **2023**, *145*, 47−52.
(18) The profile for phosphates **3a**+**3b** reaches an asymptote at 76% conversion (Figure 8b) and does not go to completion; we attribute this to the inhibitory effect of heterodimerization of phosphoric acid **1** with the succinimide byproduct during later stages of the reaction (see for the inhibitory effect of succinimide in a bromoesterification reaction). This inhibitory effect may also account for the ca. 50% conversion to phosphates **3a** and **3b** in the stoichiometric bromophosphatation reaction with phosphoric acid **1** and cyclohexene (Scheme 3), due to presumed strong heterodimerization in the absence of benzoic acid.
(19) For further instructional detail on the VTNA technique, see: (a) Burés, J. A Simple Graphical Method to Determine the Order in Catalyst. *Angew. Chem. Int. Ed.* **2016**, *55* (6), 2028−2031. (b) Burés, J. Variable Time Normalization Analysis: General Graphical Elucidation of Reaction Orders from Concentration Profiles. *Angew. Chem., Int. Ed.* **2016**, *55*, 16084−16087. (c) Martínez-Carrión, A.; Howlett, M. G.; Alamillo-Ferrer, C.; Clayton, A. D.; Bourne, R. A.; Codina, A.; Vidal-Ferran, A.; Adams, R. W.; Burés, J. Kinetic Treatments for Catalyst Activation and Deactivation Processes based on Variable Time Normalization Analysis. *Angew. Chem., Int. Ed.* **2019**, *58*, 10189−10193. (d) Nielsen, C. D. T.; Burés, J. Visual Kinetic Analysis. *Chem. Sci.* **2019**, *10*, 348−353.
(20) The (first order) time normalized different excess profiles for benzoic acid overlaid well at the beginning, but deviated at later reaction stages (see the Supporting Information). The absence of overlay at later reaction stages might result from complications of catalyst deactivation, or an interaction of the benzoic acid with succinimide.
(21) The order in benzoic acid for the bromophosphatation reaction under catalytic conditions was found to be approximately − 0.7 (see the Supporting Information).
(22) (a) Monaco, M. R.; Poladura, B.; Diaz de Los bernardos, M.; Leutzsch, M.; Goddard, R.; List, B. Activation of Carboxylic Acids in Asymmetric Organocatalysis. *Angew. Chem., Int. Ed.* **2014**, *53* (27), 7063−7067. (b) Monaco, M. R.; Pupo, G.; List, B. Phosphoric Acid Based Heterodimers in Asymmetric Catalysis. *Synlett* **2016**, *27*, 1027−1040. (c) Monaco, M. R.; Fazzi, D.; Tsuji, N.; Leutzsch, M.; Liao, S.; Thiel, W.; List, B. The Activation of Carboxylic Acids via Self-Assembly Asymmetric Organocatalysis: A Combined Experimental and Computational Investigation. *J. Am. Chem. Soc.* **2016**, *138*, 14740−14749.
(23) A control experiment was conducted to examine the reversibility of the catalyst deactivation step: phosphates **3a**+**3b** (56:44 dr) (20.7 mg, 0.024 mmol) were exposed to the standard bromoesterification conditions, without cyclohexene. HPLC monitoring indicated no bromoester **2** was formed over 8 h. Hence, formation of phosphates **3a**+**3b** must be irreversible under these conditions.
(24) This is the first example where a phosphoric acid catalyst is deactivated by nucleophilic addition to a bromonium ion. However, there are examples where other reactive electrophiles, such as epoxides and aziridines, have deactivated phosphoric acid catalysts: (a) Meyer, O.; Ponaire, S.; Rohmer, M.; Grosdemange-Billiard, C. Lewis Acid Mediated Regioselective Ring Opening of Benzylglycidol with Dibenzyl Phosphate: Short and Attractive Synthesis of Dihydroxyacetone Phosphate. *Org. Lett.* **2006**, *8* (19), 4347−4350. (b) Cytlak, T.; Saweliew, M.; Kubicki, M.; Koroniak, H. Synthesis of Trifluoromethyl γ-Aminophosphonates by Nucleophilic Aziridine Ring Opening. *Org. Biomol. Chem.* **2015**, *13* (39), 10050−10059. (c) Duarte, F.; Paton, R. S. Molecular Recognition in Asymmetric Counteranion Catalysis: Understanding Chiral Phosphate-Mediated Desymmetrization. *J. Am. Chem. Soc.* **2017**, *139*, 8886−8896.

https://doi.org/10.1021/acs.joc.5c00431
J. Org. Chem. 2025, 90, 6992−7002

(25) NMR, IR, HRMS, and HPLC data are available via a data repository: Lancaster, B. M. J.; White, A. J. P.; Tighe, C. J.; Braddock, D. C.; *Bromophosphatation as a Mode of Chiral Phosphoric Acid Catalyst Deactivation as Elucidated by Kinetic Profiling*; Imperial College Research Data Repository, 2025 DOI: 10.14469/hpc/14708.
(26) The absolute configuration of bromoester **2** was established by comparison of optical rotation data to literature: Terakado, D.; Oriyama, T. Catalytic Asymmetric Acylation of Alcohols using a Chiral 1,2-Diamine Derived from (*S*)-Proline: (1*S*,2*S*)-*trans*-1-Benzoyloxy-2-bromocyclohexane. *Org. Synth.* **2006**, *83*, 70−78.
(27) (a) Dolomanov, O. V.; Bourhis, L. J.; Gildea, R. J.; Howard, J. A. K.; Puschmann, H. *OLEX2*: A Complete Structure Solution, Refinement and Analysis Program. *J. Appl. Crystallogr.* **2009**, *42* (2), 339−341. (b) *SHELXTL v5.1*; Bruker AXS: Madison, WI, 1998. (c) Sheldrick, G. M. Crystal Structure Refinement with *SHELXL*. *Acta Crystallogr. C* **2015**, *71*, 3−8.

https://doi.org/10.1021/acs.joc.5c00431
J. Org. Chem. 2025, 90, 6992−7002